Online Deposit Material

Sample Petrography

Samples analyzed here were also studied and described by Boyce et al. (2015); the descriptions here quote those of Boyce, and include additional material on the petrography of the apatite grains and additional images of those apatite grains.

Apollo sample 10044. This is a low-K ilmenite basalt that has a Ti content lower than typical ilmenite basalts from Apollo 11. Based on its texture it was classified as coarse-grained porphyritic basalt (McGee et al., 1977) and microgabbro (e.g. Smith et al., 1970) which consists of subhedral to anhedral pyroxene, set in a matrix of plagioclase, anhedral pyroxene, and ilmenite, with minor apatite, spinel, silica, and symplectitic intergrowth. For a more detailed description of the petrography of 10044 see the Lunar sample compendium (Meyer, 2012). In this study apatite from two thin sections were examined, 10044, 12 and 10044, 644, which appear mostly as inclusions in pyroxene and oxides. The grain sizes range from < 5μm up to 200μm. Most grains are euhedral to subhedral in shape with some grains appearing as irregular-shaped aggregates.

Apatite in 10044 occurs in its mesostasis areas, adjacent to magnesian pyroxenes and closely associated with Fe-rich olivine and symplectite intergrowths (interpreted as decomposition products of the pyroxenoid pyroxferroite). The apatite grains occur as discrete euhedra and as radiating sprays. In this study, 5 apatite grains were analyzed (31 analyses total) with ranges in grain size from 20μm to 200μm.

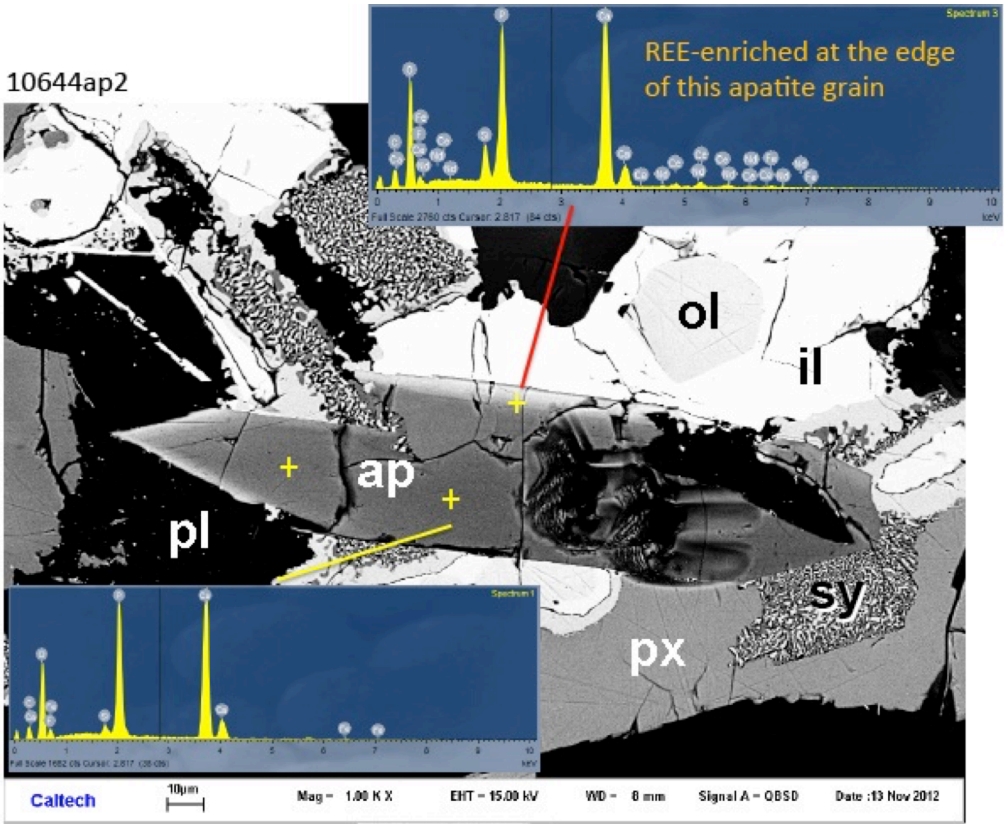

Figure S1. Apatite in basalt 10044,644 – yellow crosses on back-scattered electron (BSE) image. Euhedral apatite (ap) among pyroxene (px), ilmenite (il), plagioclase (pl), symplectite (sy), and olivine (ol). The apatite is chemically zoned, with low abundances of rare earth elements (REE) in its core, and high REE in its rim – see EDS spectra overlays.

Apollo sample 75055. This is a medium-grained ilmenite basalt that is more aluminous and less Ti rich than other Apollo 17 basalts (Rhodes et al., 1976). Based on its texture the sample has been described as subophitic (Dymek et al., 1975a; McGee et al., 1977) with tabular plagioclase intergrown with subhedral to anhedral pyroxene and ilmenite laths. For further petrographic information see the Lunar sample compendium (Meyer, 2012). In this study Apollo sample 75055,55 was analyzed.

Apatite in this sample occurs mostly as inclusions in pyroxene and oxides but some is also present in plagioclase. Apatite ranges in grain size from <5μm up to 110μm and are mostly subhedral in shape. Some grains are full euhedra, and some occur in radiating sprays of skeletal crystals with hollow centers (like some apatite from Apollo 12040 (Fig. S5). Five apatite grains have been analyzed for this study (13 analyses total), none smaller than 10μm in size.

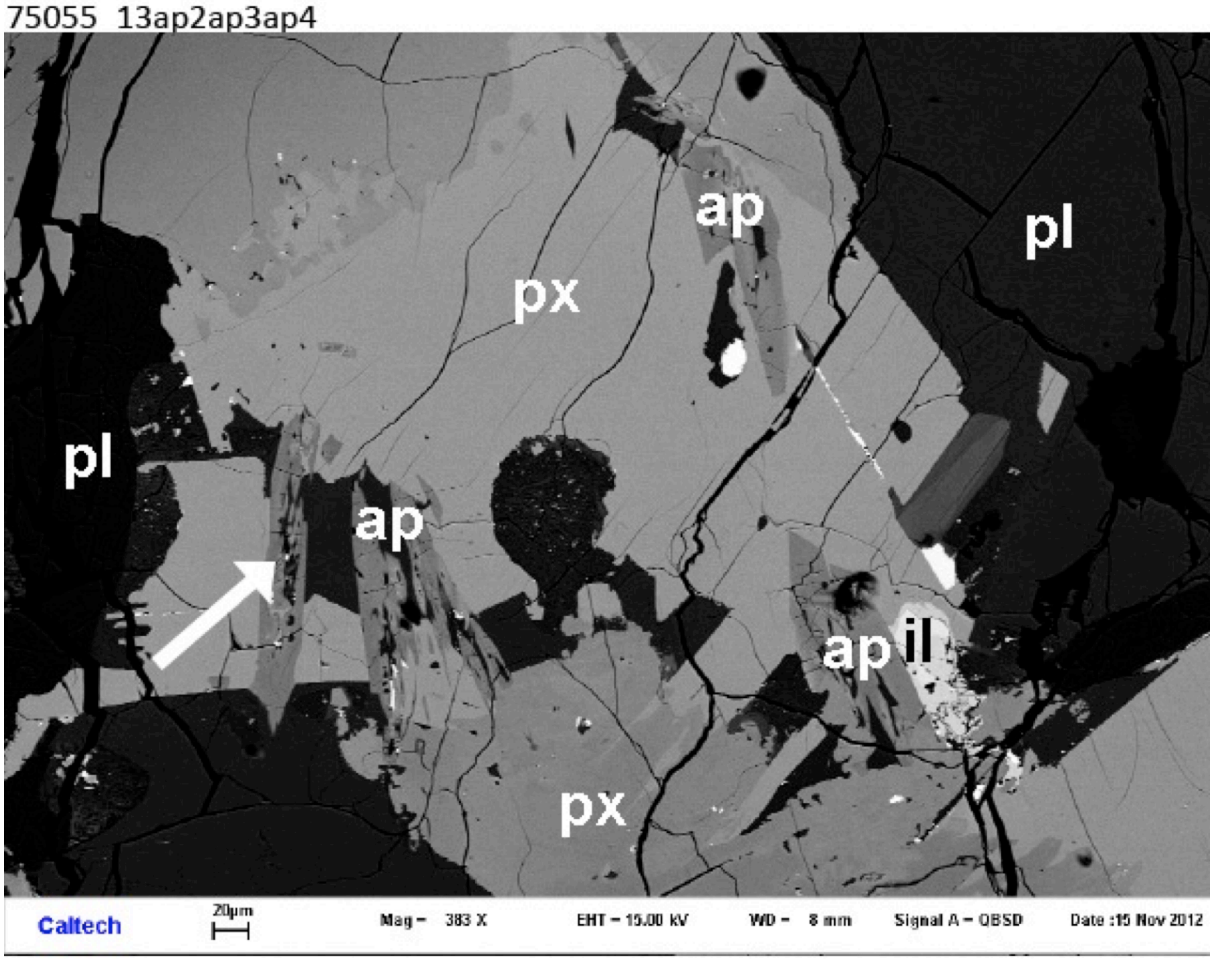

Figure S2. Apatite grains in basalt 75055,55 – back-scattered electron (BSE) image. Euhedral apatite (ap) enclosed in pyroxene (px), with plagioclase (pl), and ilmenite (il). Arrow points to a skeletal apatite crystal.

Apollo sample 12039. This is a medium-grained pigeonite basalt/microgabbro (Rhodes et al., 1977; Neal et al., 1994) and one of the most Fe-rich and Mg-poor Apollo 12 igneous rocks (Bunch et al., 1972c). Texturally, it ranges from porphyritic (McGee et al., 1977), to subophitic, to granular (Bunch et al., 1972c). Petrographically, it is composed mainly of plagioclase and pyroxene with long needles of ilmenite and tridymite cutting across the plagioclase and pyroxene. Minor troilite, tranquillityite, chromite, metal, apatite, and symplectitic intergrowths are present (Meyer, 2012).

We analyzed apatite grains in thin section 12039,42 – seventeen points in five different grains. Apatite occurs subhedral to anhedral, sometimes as long needles, with grain sizes ranging from <10μm up to 400μm long. Some grains occur as clusters and some grains show skeletal growth (Fig. S3, S4).

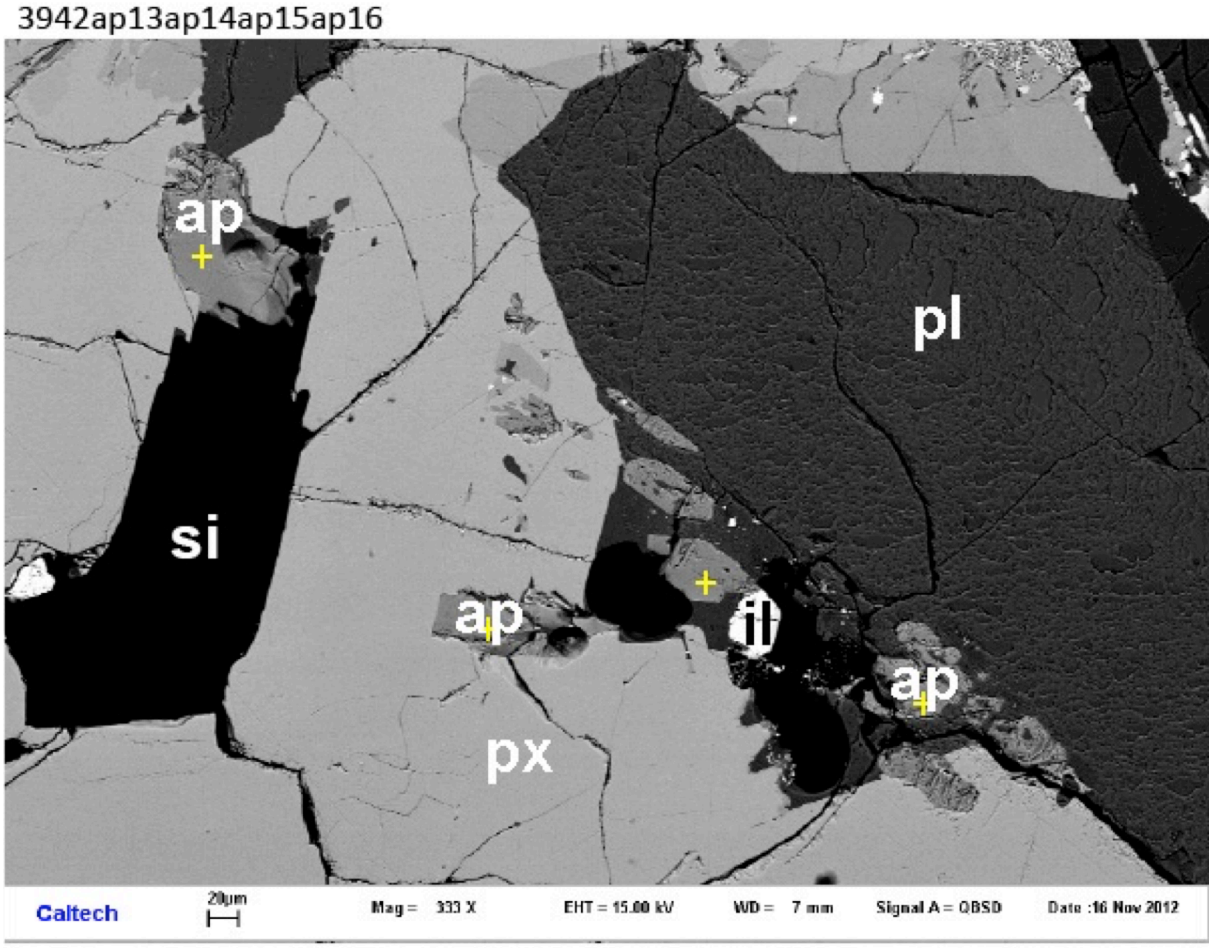

Figure S3. Apatite grains in basalt 12039,42 –yellow crosses on back-scattered electron (BSE) image. Euhedral apatite (ap) is present in pyroxene (px), and as isolated euhedra and radiating sprays associated with ilmenite (il), plagioclase (pl), and silica (si).

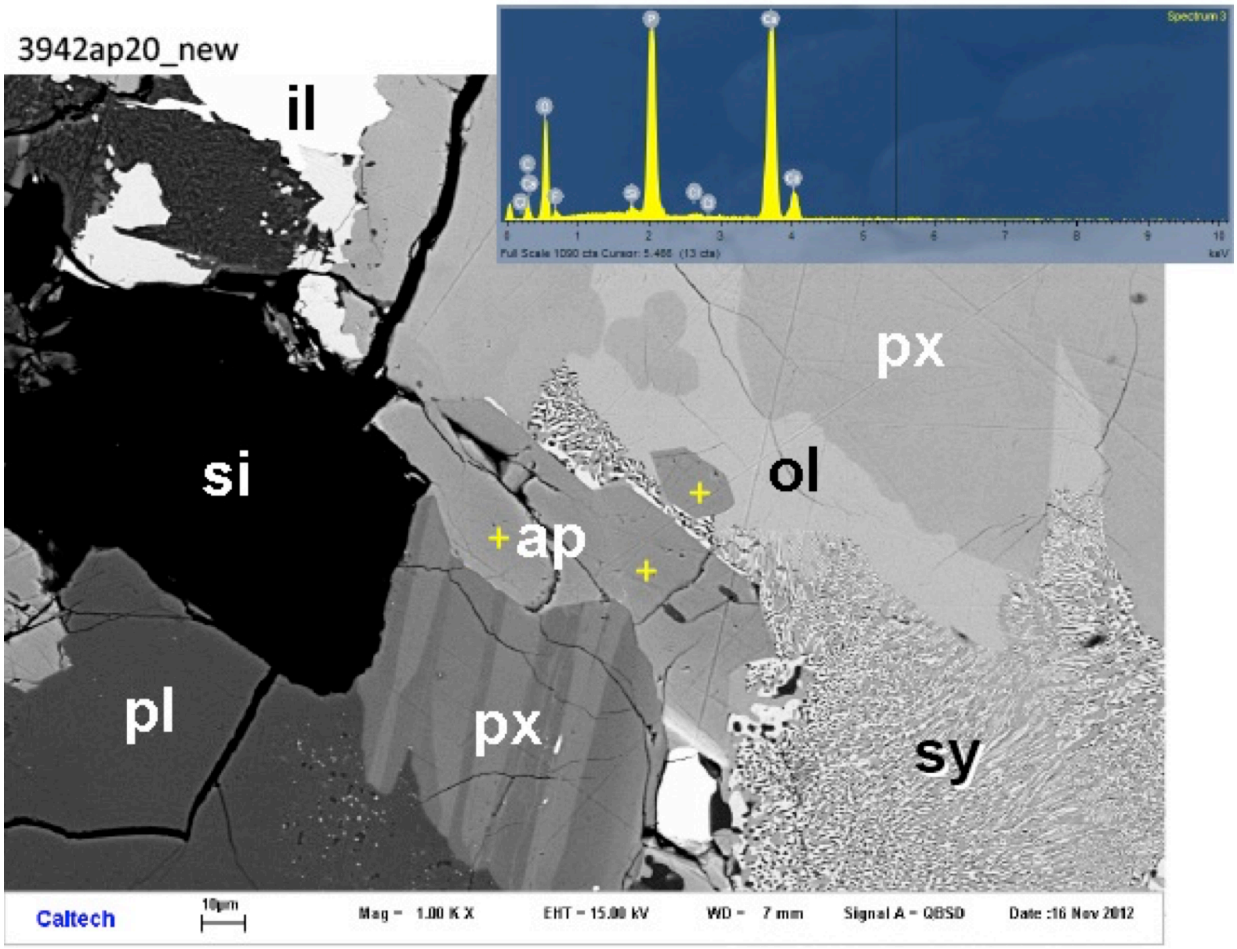

Figure S4. More apatite in basalt 12039,42 – yellow crosses on back-scattered electron (BSE) image. Inset is EDS spectrum of this apatite. Euhedral-subhedral apatite (ap) among pyroxene (px), plagioclase (pl), silica (si), symplectite (sy), and olivine (ol).

Apollo sample 12040. This is a coarse grained olivine basalt with a high proportion of mafic minerals. Texturally it is equigranular with an average grain size of 1mm (Champness et al., 1971). It is mainly composed of olivine and pyroxene with minor plagioclase, ilmenite, chromite, troilite, metal, phosphates, and alkali feldspar (Brown et al., 1971; French et al., 1972).

We analyzed three apatite grains (14 spots total) in thin section 12040,211. The apatite is mostly subhedral to anhedral and grain sizes range from <5μm to 30μm and occurs in pyroxene and plagioclase (Fig. S5), associated in some cases with merrillite (Fig. S6). Small, subhedral to euhedral apatite grains show skeletal growth with hollow centers.

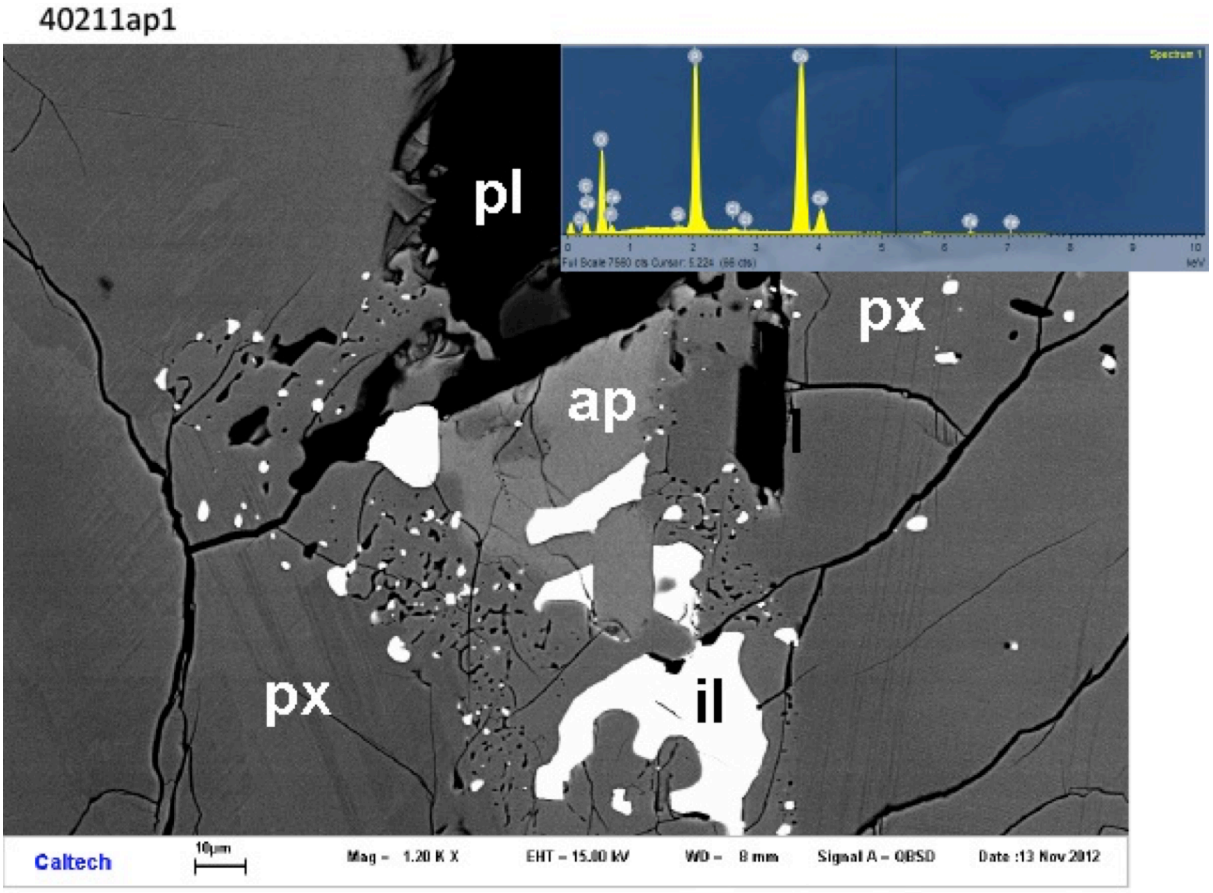

Figure S5. Apatite in basalt 12040,211 – back-scattered electron (BSE) image. Inset is EDS spectrum of this apatite. Subhedral apatite (ap) among pyroxene (px), plagioclase (pl), and ilmenite (il).

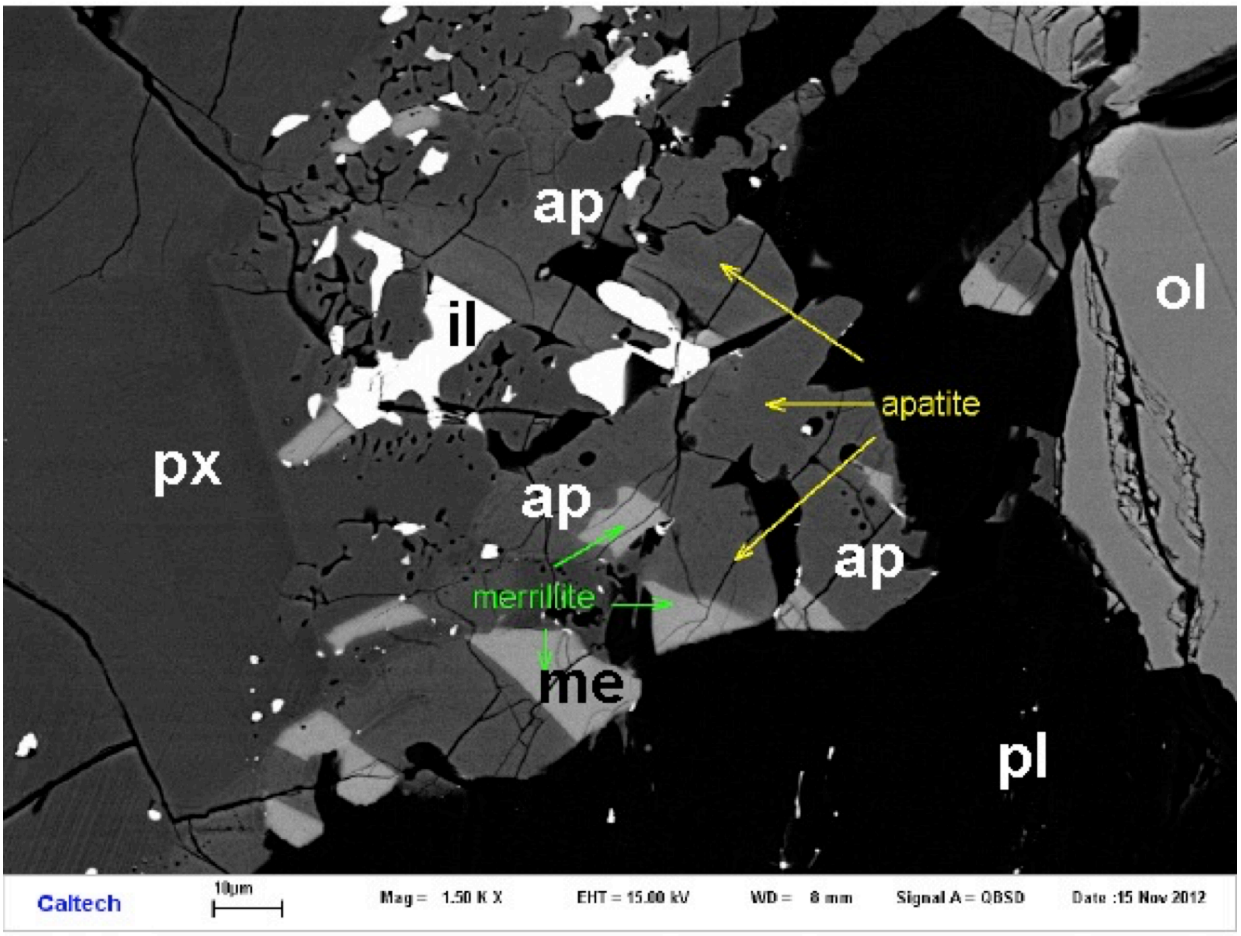

Figure S6. More apatite in basalt 12040,211 – back-scattered electron (BSE) image. Subhedral apatite (ap) intergrown with merrillite (me) among pyroxene (px), plagioclase (pl), and ilmenite (il); olivine (ol) also present.

MIL 05035. Miller Range (MIL) 05035 is a coarse grained lunar gabbroic meteorite (Joy et al., 2008). MIL 05035 consists mainly of pyroxene (54-69 vol%) with grain sizes up to 6 mm and plagioclase (17-36 vol%) with grain sizes up to 4 mm. It contains minor fayalitic olivine, ilmenite, spinel, FeS, apatite and silica, which represent crystallized products of its residual melt (Joy et al., 2008; Arai et al., 2010). MIL 05035 also contains symplectic intergrowths that are composed of silica, fayalitic olivine and hedenbergitic pyroxene (Joy et al., 2008).

In this study, a single apatite grain in the thin section MIL 05035,6 was analyzed (two points total), Figure S7.

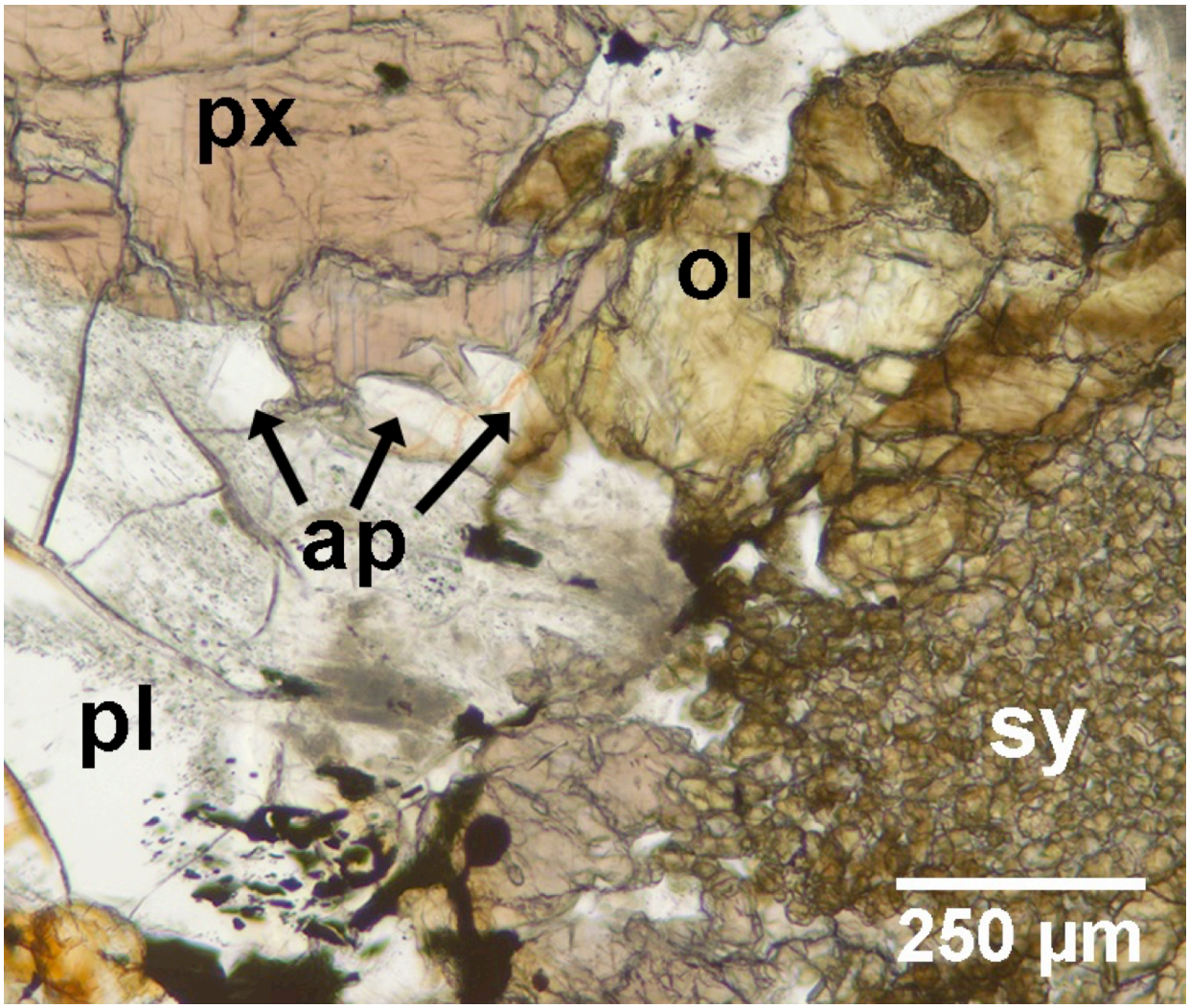

Figure S7. Apatite in basalt MIL 05035,6 – transmitted light image Euhedral apatite (ap) at boundaries of pyroxene (px), plagioclase (pl), and olivine (ol). Symplectite (sy) also present.

Methods

Measurements of H, Cl, F, and D/H were all made in the Caltech Center for Microanalysis using the Cameca 7f-GEO secondary ion mass spectrometer. Standards used for abundance measurements are those described in McCubbin et al. (2012) with the slightly revised values of Boyce et al. (2012). Isotopic measurements are reported relative to Durango apatite at $\delta^{37}Cl$ = +0.40‰ SMOC and δD = -120±5‰ VSMOW (2σ) (Greenwood et al., 2011).

Abundances of OH, F, and Cl.

Measurements of volatile abundances in lunar apatite are made by measuring $^{16}O^{1}H$, ^{18}O (reference element) ^{19}F, ^{31}P (secondary reference element), ^{32}S, and ^{35}Cl using a 0.5 nA, 10keV Cs^{+} beam at a mass resolving power of ~5500, sufficient to separate peaks of interest from all known interferences Boyce et al. (2010). Pre-analytical sputtering was performed with a 2 nA beam and 25μm x 25μm raster for 300 sec, except in cases where abundance measurements followed isotopic measurements, in which case pre-analytical sputtering was reduced to 20 sec. This was followed by 10-30 cycles of measurement with a 2μm x 2μm raster. Secondary ions were accelerated to 9keV, and those passing through a ~100μm field aperture were measured with dynamic transfer via electron multiplier, except for F and Cl which in some cases were measured with a Faraday cup. An 80% electronic gating was applied to further reduce contamination. Measurements of less than 100 ppm H_2O are very conservatively assumed to be within error of the blank for epoxy-bearing thin sections such as those studied here.

Calibration standards for H were the apatites of McCubbin et al. (2010), with the slightly revised H abundance values of Boyce et al. (2012). A San Carlos olivine standard was analyzed as a blank. The calibration curve is shown in Figure S8. The calibration is linear, with H_2O (wt%) = 2.0119*($^{16}O^{1}H/^{18}O$) – 0.0087. For this calibration, the blank is effectively 90 ppm H_2O. Our analysis of San Carlos olivine gave 28 ppm (blank subtracted), which is consistent with other analyses of 10 or 50 ppm H_2O (Kurosawa et al., 1997; Aubaud et al., 2007).

H isotopes

Measurements of H isotopes were made at low mass resolution (MRP ~ 800) with the electron multiplier, with 50-100 cycles of ~3nA, 2μm x 2μm rastered beam sputtering, preceded by 180 sec of ~3nA, 25μm x 25μm raster presputtering. Durango apatite was used as a δD standard, with a value of -120‰ VSMOW (Greenwood et al., 2011). Additional settings include: field aperture of 100μm, no dynamic transfer, electronic gating of 80% (64% by area). The instrumental background was given by analysis of San Carlos olivine; two analyses gave δD = -479±80 and -245±80 ‰, at a total H_2O abundance of < 50 ppm. Correction for this blank is only significant for the water-poor apatite in sample 12040 (Table S1).

Figure S8. Calibration curve for H_2O abundances in apatite; H abundance measured as ion counts for p $^{16}O^{1}H$, which was clearly resolved from those of ^{17}O. Equation is linear least-squares correlation line; uncertainties from counting statistics are smaller than the symbols.

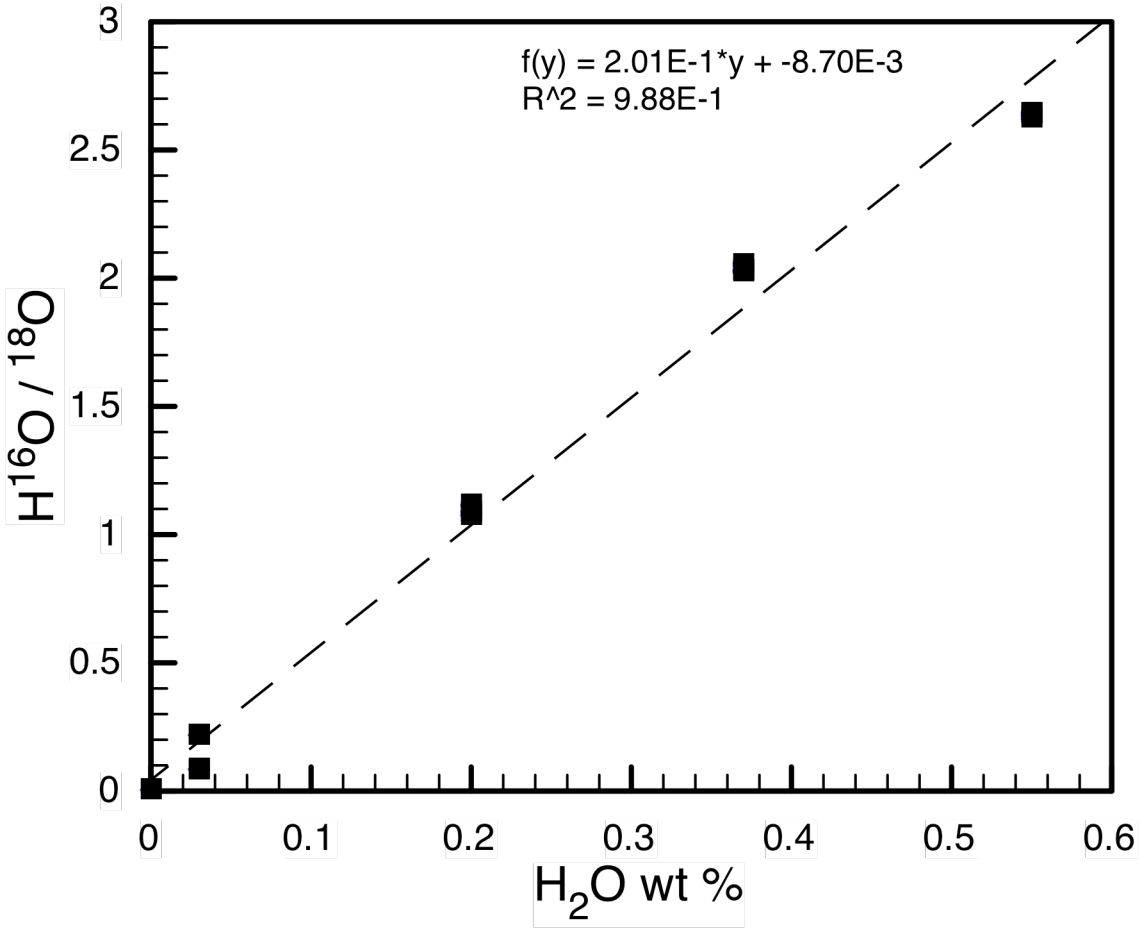

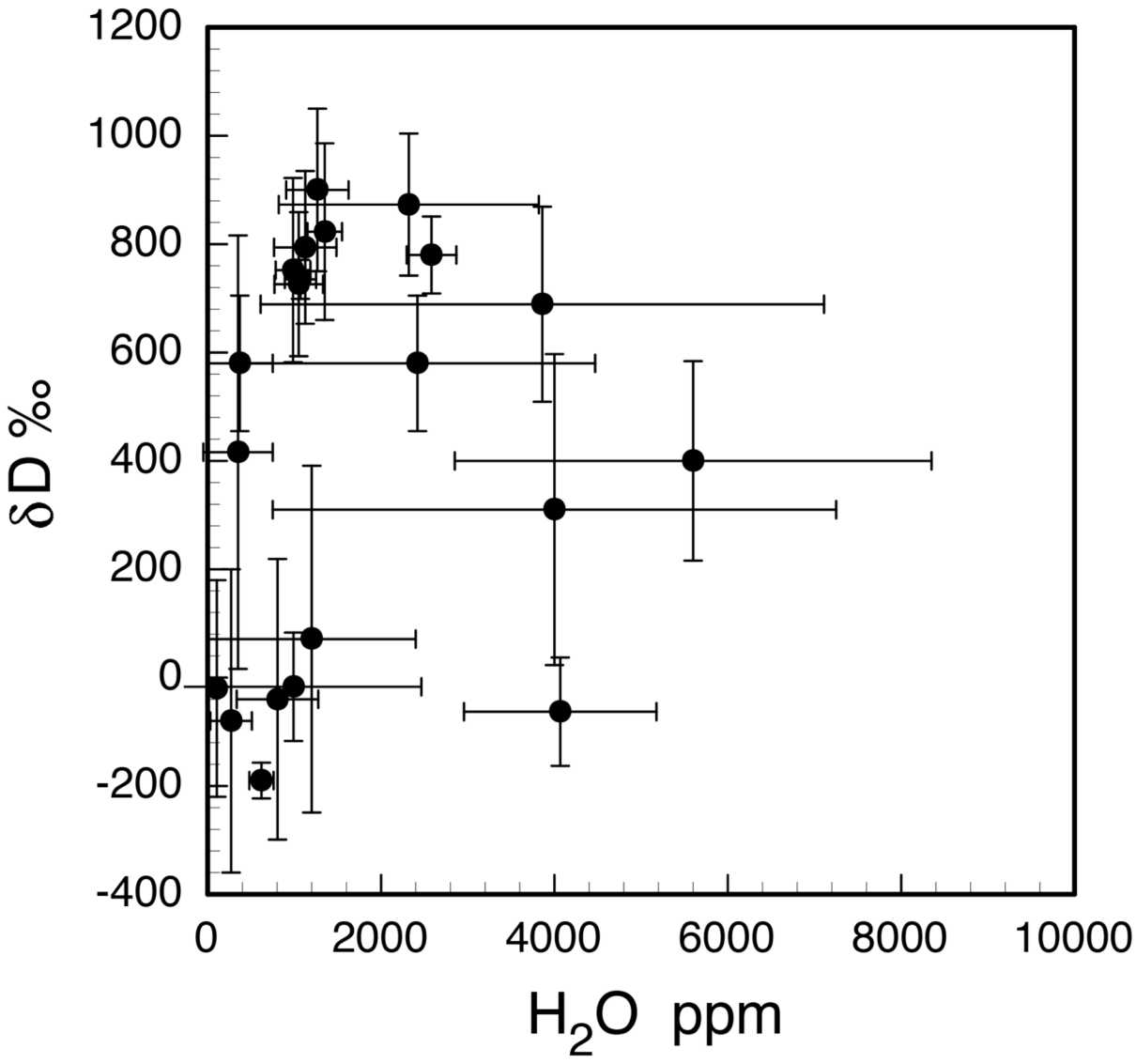

Figure S9. H_2O abundances and δD values in apatite, averages by sample and reference. Data and sources in Table S2.

Supplemental Tables

Table S1. New data generated in this study

sample	section	grain	H2O (ppm)	H2O 2σ (ppm)	δD meas. ‰	δD corr.* ‰	δD 2σ ‰	Cl (ppm)	Cl 2σ (ppm)	δ^{37}Cl ‰	δ^{37}Cl ‰ 2σ	Basalt Type
10044	**12**	**10**	1105	29	933	932	31	365	104	9	3	High Ti
10044	**12**	**1a**	728	27	954	953	27	292	11	6	3	High Ti
10044	**12**	**1b**	—	—	—		—	—	—	6	4	High Ti
10044	**12**	**1c**	1220	30	781	781	23	300	11	2	4	High Ti
10044	**644**	**2**	877	26	536	536	57	250	10	11	3	High Ti
10044	**644**	**8**	421	22	—		—	3976	122	15	3	High Ti
10044	**644**	**4a**	826	25	606	605	33	219	10	12	3	High Ti
10044	**644**	**4b**	1155	29	702	702	28	479	16	12	3	High Ti
75055	**55**	**1**	604	23	621	621	35	398	14	8	3	High Ti
75055	**55**	**2**	1225	35	794	794	26	485	16	6	3	High Ti
75055	**55**	**3**	1241	30	968	967	27	334	12	14	3	High Ti
75055	**55**	**4**	1430	34	794	794	26	410	14	6	3	High Ti
75055	**55**	**101**	—	—	—		—	—	—	5	3	High Ti
12039	**42**	**4**	1996	43	720		30	928	29	18	3	Low Ti
12039	**42**	**6**	2379	47	830		31	477	16	17	3	Low Ti
12039	**42**	**10**	—	—	—		—	—	—	16	3	Low Ti
12039	**42**	**11**	—	—	—		—	—	—	17	3	Low Ti
12039	**42**	**17a**	2784	95	729		28	1157	36	17	3	Low Ti
12039	**42**	**17b**	2916	57	698		28	665	21	16	3	Low Ti
12040	**211**	**1**	105	21	9	-20	200	15884	489	17	3	Low Ti
12040	**211**	**4**	3	20	14	-900	150	2689	83	13	3	Low Ti
12040	**211**	**5**	16	20	-150	-340	35	3388	104	14	4	Low Ti
MIL 05035	**—**	**1**	—	—	—		—	—	—	-4	2	Low Ti

* Corrected for spallation deuterium, based on published cosmic ray exposure ages.

Table S2 - Sample averages, by reference

sample	ref	H2O (ppm)	H2O 2σ (ppm)	δD corr.* ‰	δD 2σ ‰	px Mg# (max)	px Mg# (min)	Mg#(Min) / Mg#(Max)	ol Mg# (max)	ol Mg# (min)	Mg#(Min) / Mg#(Max)	ref	CRE Age m.y.	Basalt Type
10044	This Work	985	201	752	170	80	4	0.050	x	x	x	Meyer12	80	High Ti
10044	Greenwood11	1050	280	613	40	80	4	0.050	x	x	x	Meyer12	80	High Ti
10044	Barnes13	1240	500	726	260	80	4	0.050	x	x	x	Meyer12	80	High Ti
10058	Tartese13	1350	400	823	163	75	2	0.027	x	x	x	Meyer12	70	High Ti
12039	This Work	2582	286	780	71	65	3	0.046	x	x	x	Meyer12		Low Ti
12039	Tartese13	2320	1500	873	130	65	3	0.046	x	x	x	Meyer12		Low Ti
12039	Greenwood11	3860	3250	690	360	65	3	0.046	x	x	x	Meyer12		Low Ti
12040	This Work	105	21	-20	200	70	50	0.714	54	38	0.704	Meyer12	285	Low Ti
12064	Barnes13	1265	360	900	150	65	2	0.031	x	x	x	Meyer12		Low Ti
14053	Greenwood11	620	140	-190	33	70	2	0.029	x	x	x	Meyer12		High Al
14053	Pernet-Fisher14	990	1475	-17	100	70	2	0.029	x	x	x	Meyer12		High Al
15058	Tartese13	370	380	580	125	68	6	0.088	x	x	x	Meyer12		Low Ti
15386	Tartese14b	350	400	416	400	85	5	0.059	x	x	x	Meyer12		KREEP
15555	Tartese13	2420	2050	600	200	65	2	0.031	67.000	2.000	0.030	Meyer12		Low Ti
72275	Tartese14b	270	240	-80	280	78	12	0.154	x	x	x	Meyer12		KREEP
75055	This Work	1125	360	794	141	70	3	0.043	x	x	x	Meyer12		High Ti
75055	Greenwood11	1070	180	735	36	70	3	0.043	x	x	x	Meyer12		High Ti
Kalahari	Tartese14a	1200	1200	71	320	85	10	0.118	52.000	0.000	0.000	Sokol08		VLT
LAP 04841	Tartese13	5600	2750	400	180	60	3	0.050	68.000	0.000	0.000	Righter13	55	Low Ti
MIL 05035	Tartese13	4000	3250	310	285	50	3	0.060	x	x	x	Righter13		Low Ti
NWA 773 gabbro	Tartese14b	1415	1300	-40	260	75	65	0.867	69	63	0.913	Jolliff03	160	KREEP
NWA 4472 clast	Tartese14b	4100	2200	-63	100	85	30	0.353	47.000	44.000	0.936	Joy11		KREEP

* Corrected for spallation deuterium, based on published cosmic ray exposure ages.

Supplemental References

Arai, T., Hawke, B.R., Giguere, T.A., Misawa, K., Miyamoto, M., and Kojima, H. (2010) Antarctic lunar meteorites Yamato-793169, Asuka-88175, MIL 05035, and MET 01210 (YAMM): Launch pairing and possible cryptomare origin. Geochimica Cosmochimica Acta, 74, 2231-2248.

Aubaud, C., Withers, A.C., Hirschmann, M.M., Guan, Y., Leshin, L.A., Mackwell, S.J., and Bell, D.R. (2007) Intercalibration of FTIR and SIMS for hydrogen measurements in glasses and nominally anhydrous minerals. American Mineralogist, 92(5-6), 811-828.

Boyce, J.W., Eiler, J.M., and Channon, M.C. (2012) An inversion-based self-calibration for SIMS measurements: Application to H, F, and Cl in apatite. American Mineralogist, 97, 1116-1128.

Boyce, J.W., Liu, Y., Rossman, G.R., Guan, Y., Eiler, J.M., Stolper, E.M., and Taylor, L.A. (2010) Lunar apatite with terrestrial volatile abundances. Nature, 466, 466-469.

Boyce, J.W., Treiman, A.H., Guan, Y., Ma, C., Eiler, J.M., Gross, J., Greenwood, J.P., and Stolper, E.M. (2015) The chlorine isotopic fingerprint of the lunar magma ocean. Science Advances, 1, e1500380.

Brown, G.M., Emeleus, C.H., Holland, J.G., Peckett, A., and Phillips, R. (1971) Picrite basalts, ferrobasalts, feldspathic norites, and rhyolites in a strongly fractionated lunar crust. Lunar Science Conference 2nd, p. 583-600.

Bunch, T.E., Keil, K., and Prinz, M. (1972c) Mineralogy, petrology and chemistry of lunar rock 12039. Meteoritics, 7, 245-255.

Champness, P.E., Dunham, A.C., Gibb, F.G.F., Giles, H.N., MacKenzie, W.S., Stumpel, E.F., and Zussman, J. (1971) Mineralogy and petrology of some Apollo 12 lunar samples. Lunar and Planetary Science Conference 2nd, p. 359-376.

Dymek, R.F., Albee, A.L., and Chodos, A.A. (1975a) Comparative mineralogy and petrology of Apollo 17 mare basalts: Samples 70215, 71055, 74255, and 75055. 6th Lunar and Planetary Science Conference.

French, B.M., Walter, L.S., Heinrich, K.F.J., Loman, P.D., Doan, A.S., and Adler, I. (1972) Composition of major and minor minerals in five Apollo 12 crystalline rocks. NASA.

Greenwood, J.P., Itoh, S., Sakamoto, N., Warren, P.H., A, T.L., and Yurimoto, H. (2011) Hydrogen isotope ratios in lunar rocks indicate delivery of cometary water to the Moon. Nature Geoscience, 4, 79-82.

Jolliff, B.L., Korotev, R.L., Zeigler, R.A., and Floss, C. (2003) Northwest Africa 773: Lunar mare breccia with a shallow-formed olivine-cumulate component, inferred very-low-Ti (VLT) heritage, and a KREEP connection. Geochimica et Cosmochimica Acta, 67(24), 4857-4879.

Joy, K.H., Burgess, R., Hinton, R., Fernandes, V., Crawford, I.A., Kearsley, A., and Irving, A. (2011) Petrogenesis and chronology of lunar meteorite Northwest Africa 4472: A KREEPy regolith breccia from the Moon. Geochimica et Cosmochimica Acta, 75(9), 2420-2452.

Joy, K.H., Crawford, I.A., Anand, M., Greenwood, R.C., Franchi, I.A., and Russell, S.S. (2008) The petrology and geochemistry of Miller Range 05035: A new lunar gabbroic meteorite. Geochimica Cosmochimica Acta, 72, 3822-3844.

Kurosawa, M., Yurimoto, H., and Sueno, S. (1997) Patterns in the hydrogen and trace element compositions of mantle olivines. Physics and Chemistry of Minerals, 24(6), 385-395.

McCubbin, F.M., Hauri, E.H., Elardo, S.M., E, V.K.K., J, W., and Shearer, C.K. (2012) Hydrous melting of the martian mantle produced both depleted and enriched shergotites. Geology, 40(8), 683-686.

McCubbin, F.M., Steele, A., Hauri, E.H., Nekvasil, H., Yamashita, S., and Hemley, R.J. (2010) Nominally hydrous magmatism on the Moon. Proceedings of the National Academy of Sciences, 107, 11223-11228.

McGee, P.E., Warner, J.L., and Simonds, C.H. (1977) Introduction to the Apollo collections. Part 1: Lunar igneous rocks. NASA STI/Recon Technical Report.

Meyer, C. (2012) Lunar Sample Compendium. NASA.

Neal, C.R., Hacker, M.D., Snyder, G.A., Taylor, L.A., Liu, Y.-G., and Schmitt, R.A. (1994) Basalt generation at the Apollo 12 site, Part 2: Source heterogeneity, multiple melts and crustal contamination. . Meteoritics, 29, 349-361.

Pernet-Fisher, J., Howarth, G., Liu, Y., Chen, Y., and Taylor, L. (2014) Estimating the lunar mantle water budget from phosphates: Complications associated with silicate-liquid-immiscibility. Geochimica et Cosmochimica Acta, 144, 326-341.

Rhodes, J.M., Blanchard, D.P., Dungan, M.A., Brannon, J.C., and Rodgers, K.V. (1977) Chemistry of Apollo 12 mare basalts: Magma types and fractionation processes. . 8th Lunar and Planetary Science Conference, p. 1305-1338.

Rhodes, J.M., Wiesmann, H., Rodgers, K.V., Brannon, J.C., Bansal, B.M., and Hubbard, N.J. (1976) Chemistry, classification, and petrogenesis of Apollo 17 mare basalts. 7th Lunar Science Conference, 2, p. 1467-1489, Houston, Texas.

Righter, K., and Gruener, J. (2013) The Lunar Meteorite Compendium. NASA Johnson Space Center, NASA Johnson Space Center.

Smith, J.V., Anderson, A.T., Newton, R.C., Olsen, E.J., Crewe, A.V., Isaacson, M.S., and Johnson, D. (1970) Petrologic history of the moon inferred from petrography, mineralogy and petrogenesis of Apollo 11 rocks. Apollo 11 Lunar Science Conference 1, p. 897.

Sokol, A., Fernandes, V., Schulz, T., Bischoff, A., Burgess, R., Clayton, R., Münker, C., Nishiizumi, K., Palme, H., and Schultz, L. (2008) Geochemistry, petrology and ages of the lunar meteorites Kalahari 008 and 009: New constraints on early lunar evolution. Geochimica et Cosmochimica Acta, 72(19), 4845-4873.